Kinetic Modeling of Fe-BEA as NH_3-SCR Catalyst—Effect of Phosphorous

Soran Shwan, Louise Olsson, and Magnus Skoglundh
Competence Centre for Catalysis, Chalmers University of Technology, SE 412 96 Gothenburg, Sweden

Jonas Jansson
Volvo Group Trucks Technology, SE 405 08, Gothenburg, Sweden

DOI 10.1002/aic.14638
Published online October 9, 2014 in Wiley Online Library (wileyonlinelibrary.com)

The focus of this work is to investigate whether a previously developed microkinetic deactivation model for hydrothermally treated Fe-BEA as NH_3-SCR catalyst can be applied to describe chemical deactivation of Fe-BEA due to phosphorous exposure. The model describes the experiments well for Fe-BEA before and after phosphorous exposure by decreasing the site density, representing deactivation of sites due to formation of metaphosphates blocking the active iron sites, while the kinetic parameters are kept constant. Furthermore, the results show that the activity for low-temperature selective catalytic reduction (SCR) is very sensitive to loss of active monomeric iron species due to phosphorous poisoning compared to high-temperature SCR. Finally, the ammonia inhibition simulations show that exposure to phosphorous may affect the internal transport of ammonia between ammonia storage sites buffering the active iron sites, which results in a lower SCR performance during transient conditions. © 2014 American Institute of Chemical Engineers *AIChE J*, 61: 215–223, 2015
Keywords: microkinetic model, phosphorous exposure, Fe-BEA, deactivation, poisoning, NH_3-SCR

Introduction

With an increasing globalization and a growing transport sector, the interest for diesel and learn-burn gasoline engines has increased due to higher fuel-efficiency compared to conventional gasoline engines, operating under stoichiometric conditions. Selective catalytic reduction with ammonia (NH_3-SCR) is presently the most commonly used and effective method to eliminate nitrogen oxides (NO_X) from lean exhausts[1] where copper-[2–7] and iron-[1,3,8–11] exchanged zeolites have proven to be very active and promising alternatives to the commonly used vanadia-based NH_3-SCR catalysts.[1,12,13]

Chemical poisoning and thermal stability are two of the most important challenges arising, when using zeolite-based materials in aftertreatment systems for diesel and lean-burn gasoline engines.[1,14–16] Recently, we have studied the hydrothermal stability and tolerance against phosphorous poisoning of iron-exchanged zeolite BEA (Fe-BEA) as NH_3-SCR catalyst.[14–19] In particular, we have studied the dynamics of the iron species providing the active sites for NH_3-SCR during hydrothermal treatment and gas phase exposure to phosphorous. The results from the chemical poisoning study, where Fe-BEA was exposed to 10 and 50 ppm phosphoric acid between 14 and 48 h, show that the deactivation proceeds in two steps; (1) short time of exposure results mainly in formation of phosphorous pentoxides, P_2O_5, not considerably affecting the NO_X conversion, and (2) longer time of exposure results in relatively high formation of metaphosphates, PO_3^-, which results in a significant decrease in NO_X conversion by replacing hydroxyl groups with metaphosphates on the active iron sites.[14] Furthermore, it was found that the degree of deactivation under those conditions is strongly dependent on the exposure time and not on the concentration of phosphoric acid in the exposing gas, which indicates that the formation of metaphosphates proceeds via a surface reaction and is not limited by the supply of phosphoric acid in that particular study.

It has been pointed out by, for example, Bartholomew[20] that understanding the fundamental deactivation mechanisms is very important for designing new catalysts and optimizing operation conditions for catalytic processes, hence the need of kinetic models that can explain the main mechanisms for catalyst deactivation. Based on the experimental results from our hydrothermal treatment studies, a multisite kinetic deactivation model of Fe-BEA was developed with focus on the dynamics of the active iron sites before and after hydrothermal treatment.[16] The model is able to predict the deactivation experiments well by decreasing the site density and keeping the kinetic parameters constant. To our knowledge, the model presented in this study is the first kinetic model that describes chemical poisoning of zeolites used in NH_3-SCR.

The objective of this study is to investigate whether the previously developed microkinetic deactivation model for NH_3-SCR over hydrothermally treated Fe-BEA[16] can

Additional Supporting Information may be found in the online version of this article.

Correspondence concerning this article should be addressed to S. Shwan at soran@chalmers.se.

Table 1. Site Density and Desorption Energy of NH_3 for All Samples

Sample	W ($\times 10^{-5}$)[a]	$Z_{Br,1}$ ($\times 10^{-5}$)[a]	$Z_{Br,2}$ ($\times 10^{-5}$)[a]	$Fe_{M,1\ or\ 2}$ ($\times 10^{-5}$)[a]	Fe_D ($\times 10^{-5}$)[a]	Fe_P ($\times 10^{-5}$)[a]	Act. Energy E_a (kJ/mol)[b]
Fresh	2066	547	4.434	52.29	16.31	10.31	79.7
14 h (10 ppm)	1406	660	4.434	46.14	12.74	10.31	78.3
24 h (10 ppm)	1406	595	4.434	45.94	12.74	8.55	76.5
48 h (10 ppm)	1406	552	4.434	39.55	10.54	6.79	79.2
14 h (50 ppm)	1406	661	4.434	48.34	14.06	10.31	78.0
24 h (50 ppm)	1406	650	4.434	46.01	14.06	8.11	76.7
48 h (50 ppm)	2066	525	4.434	41.75	11.21	6.35	78.7

[a]Unit: mol/m^2
[b]Desorption energy of NH_3 from Brønsted acid sites ($Z_{Br,1}$) for Reaction 2 (r_2)

be applied to describe chemical deactivation of Fe-BEA due to phosphorous exposure.[14] The focus is paid on the dynamics of the active iron species and prediction of the decreased catalytic activity due to phosphorous poisoning of the active iron sites to gain further understanding of the deactivation mechanisms of Fe-BEA as NH_3-SCR catalyst.

Experimental Methods

Sample preparation and phosphorous exposure

Seven monolith substrates were coated with about 700 mg of washcoat of 1 wt % Fe-BEA catalyst, which was prepared using incipient wetness impregnation. Further details of the catalyst preparation can be found in Ref. 14.

Six catalysts were exposed to evaporated diluted phosphoric acid solutions using an ageing reactor and one sample was kept untreated (fresh) for comparison with the samples exposed to phosphorous. Phosphoric acid was mixed with distilled water in the water feed system of the ageing reactor. The diluted phosphoric acid solution was thereafter introduced separately to the preheater via a controlled evaporator mixer system (CEM, Bronkhorst Hi-Tech) where it was mixed with inert gas (nitrogen) and heated to 350°C before fed to the ageing reactor. Three of the samples were exposed to 10 ppm H_3PO_4, and the remaining three samples were exposed to 50 ppm of H_3PO_4 for 14, 24, and 48 h. The samples exposed to 10 ppm H_3PO_4 are referred to as 14 h (10 ppm), 24 h (10 ppm), and 48 h (10 ppm), and the samples exposed to 50 ppm H_3PO_4 are referred to as 14 h (50 ppm), 24 h (50 ppm), and 48 h (50 ppm) in Table 1 and Figures 1–4. In this article, only the simulated results from the samples exposed to 10 ppm phosphoric acid are shown. However, the changes in the kinetic parameters are shown for both exposing concentrations. Further details about the ageing reactor and the phosphorous exposure can be found in Ref. 14.

Flow reactor system

Temperature-programmed desorption of ammonia and nitric oxide (NH_3- and NO-TPD, respectively), NO- and NH_3-oxidation, SCR of NO_X with ammonia (NH_3-SCR) and NH_3 inhibition experiments were used to evaluate the kinetic model. NO and/or NH_3 (400 ppm) was used in different combinations with 8% O_2 and 5% H_2O between 150 and 500°C using Ar as inert gas.

The NH_3- and NO-TPD experiments, and the experiments for evaluation of the catalytic performance (NH_3- and NO-oxidation, NH_3-SCR, and NH_3 inhibition experiments) were performed using a continuous gas flow reactor system, which is described in more detail in Refs. 2,14, and 16.

Further details about the flow reactor measurements can be found in Ref. 14.

Kinetic Modeling

Reactor model

AVL BOOST[21] was used in combination with user-defined files in FORTRAN to conduct kinetic modeling.[16,18,22] The ideal gas law is applied and all gas properties are evaluated depending on the temperature, pressure, and gas composition. Mass-transfer from the gas bulk to the surface was included, while mass-transfer in the washcoat was not modeled. In a previous study by Olsson et al.,[23] the effect of mass-transfer in the washcoat was examined for NH_3-SCR over Cu-ZSM-5 by reducing the washcoat thickness with a factor of two and simultaneously decrease the total flow with a factor of two. The same conversion was obtained over the entire temperature interval, which suggests that there are no mass-transport limitations in the washcoat. However, at medium to higher temperatures full conversion was reached and conclusions regarding the mass-transfer could not be made. In several previously reported SCR models, the mass-transfer in the washcoat was neglected.[23–26] There is still a possibility that there are mass-transfer limitation in the washcoat under our reaction conditions, and therefore, the received parameters should be considered as apparent rate parameters. Furthermore, in an experimental study by Silver et al.,[27] axial gradients of phosphorous were observed after exposure to phosphorous-doped diesel fuel exhaust gases of an iron-exchanged zeolite. However, using X-ray Photoelectron Spectroscopy (XPS) at three locations on our phosphorous poisoned catalyst, we did not observe any gradients. To keep the model as simple as possible phosphorous gradients are not taken into consideration. Further details about the assumptions made for the reactor model can be found in Refs. 16 and 22.

Kinetic model

A kinetic model for temperature-dependent reaction rates was developed. To simulate and capture the temperature dependence, the Arrhenius equation is used for the rate constants, where all kinetic parameters are taken from our previously developed kinetic deactivation model for hydrothermally treated H-BEA and Fe-BEA used as NH_3-SCR catalysts.[16] For a more thorough description of the kinetic model, reaction rates, and parameter fitting, see Ref. 16. Furthermore, all reaction rates and parameters used for the simulations can be found in the Supporting Information of this paper (Section S1). However, a brief description of the kinetic model is presented below.

NH_3 and NO Adsorption. The previously developed deactivation model includes reaction steps for adsorption and

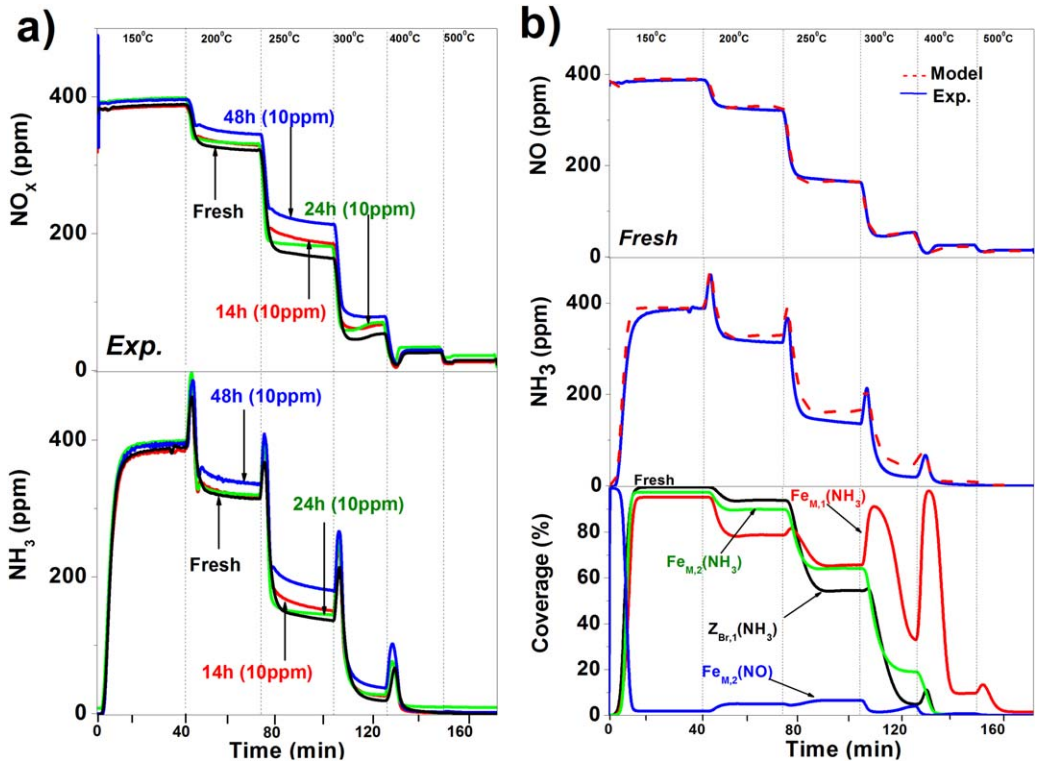

Figure 1. Evolution of NO and NH_3 concentrations during NH_3-SCR experiments over Fe-BEA.

(a) Catalysts exposed to 10 ppm H_3PO_4 for 14, 24, and 48 h compared to a fresh sample. (b) Measured and calculated NO and NH_3 outlet concentrations during NH_3-SCR experiments for the fresh Fe-BEA sample with the surface coverage of NO and NH_3 over sites, $Z_{Br,1}$, $Fe_{M,1}$, and $Fe_{M,2}$. The samples were exposed to 400 ppm NO, 8% O_2, and 5% H_2O at 150, 200, 250, 300, 400, and 500°C. The total flow rate was 3500 mL/min and Ar was used as balance. [Color figure can be viewed in the online issue, which is available at wileyonlinelibrary.com.]

desorption of ammonia over zeolite and iron sites.[16] The zeolite model contains sites for weakly (denoted W) and strongly (denoted $Z_{Br,1}$) bound ammonia. Furthermore, Brandenberger et al.[28] have concluded that at lower temperatures (150–300°C), monomeric iron species provide the governing site for NH_3-SCR, while at higher temperatures (400–500°C), the reaction is governed by dimeric iron species. Therefore, the model contains sites for ammonia adsorption over monomeric iron species to predict transient conditions accurately at lower temperatures. It has been shown by Hoj et al.[29] that two ammonia molecules can adsorb on each iron site, and therefore, the monomeric iron site, Fe_M, is defined as two sites, denoted $Fe_{M,1}$ and $Fe_{M,2}$, with equal site density, where one ammonia molecule can be bound to each site. A spillover mechanism is included in the model where ammonia is assumed to spillover from the main zeolite storage site ($Z_{Br,1}$) to one of the monomeric iron sites ($Fe_{M,1}$). However, the spillover rate is independent of the site density. Furthermore, the model includes surface coverage-dependent activation energies for all NH_3 adsorption sites according to the expression $E_{a,i}=E_{a,i}(0)(1-\alpha_{i,k}\theta_k)$.

For the model to be able to describe transient conditions, especially at lower temperatures where ammonia inhibition is observed, NO adsorption and desorption steps need to be included in the model, and therefore, NO is assumed to adsorb on both Brønsted and monomeric iron sites. NO is set to adsorb on the Brønsted site denoted $Z_{Br,2}$, where $Z_{Br,2}$ represents a small fraction of the main Brønsted site $Z_{Br,1}$. For the iron sites, NO is assumed to adsorb on one of the monomeric iron sites, $Fe_{M,2}$. A more detailed description and discussion about the assumptions in the model can be found in Ref. 16.

NH_3 and NO Oxidation. Both NH_3- and NO-oxidation are modeled as direct reactions, dependent on the corresponding site density, but not between adsorbed species as no transient effects were observed during NH_3- or NO-oxidation.[16] However, we would like to emphasize that this does not mean that the reactions do not proceed between adsorbed species, but only a simplification for a global kinetic step. For the pure zeolite, both the NH_3 and NO oxidation reaction are set to proceed over site $Z_{Br,2}$. For the iron-exchanged zeolites, dimeric iron has been shown to be the governing site for NH_3-oxidation[28] and iron particles, Fe_2O_3, for NO-oxidation. Hence ammonia is assumed to be oxidized over dimeric iron sites (denoted Fe_D) and NO-oxidation is modeled to proceed over Fe_2O_3 particle sites (denoted Fe_P)

NH_3-SCR. The standard SCR reaction for zeolite BEA, is modeled to proceed between adsorbed NO and NH_3 species on the Brønsted sites, $Z_{Br,2}$ and $Z_{Br,1}$, respectively. Furthermore, it has been shown experimentally by Brandenberger et al.[28] that for Fe-ZSM-5, the low-temperature (150–300°C) NH_3-SCR reaction is mainly governed over monomeric iron species and at high temperatures (400–500°C), the reaction is governed by dimeric iron species. Therefore, the NH_3-SCR model for Fe-BEA includes two reactions; (1) the standard SCR reaction between NO and NH_3 adsorbed on monomeric iron species, $Fe_{M,2}$ and $Fe_{M,1}$, respectively, and (2) a second SCR step over dimeric iron species, Fe_D. Furthermore, it is very difficult to fit adsorption parameters for the dimeric iron sites at higher

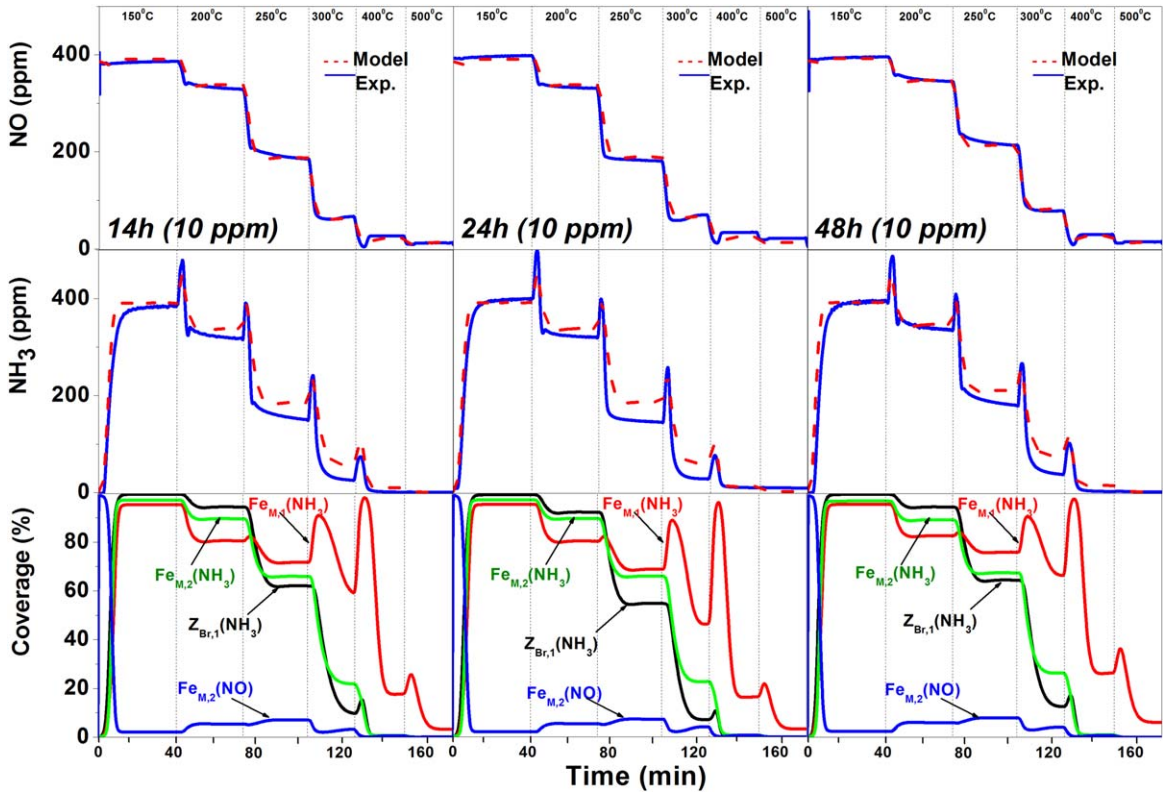

Figure 2. Measured and calculated NO and NH_3 outlet concentration during NH_3-SCR experiments for all Fe-BEA samples exposed to 10 ppm of H_3PO_4 with the surface coverage of NO and NH_3 over sites, $Z_{Br,1}$, $Fe_{M,1}$, and $Fe_{M,2}$.

[Color figure can be viewed in the online issue, which is available at wileyonlinelibrary.com.]

temperatures. As previously shown,[16,18] NH_3 inhibition experiments have not shown any significant inhibition effects for temperatures above 300°C, hence, the second SCR reaction is modeled as a direct reaction over the dimeric iron sites. Again, we would like to emphasize that this does not mean that the reaction does not proceed between adsorbed species, this is only a simplification for a global kinetic step. The activation energies for the two SCR reactions over Fe-BEA are fixed according to the experimental values found by Brandenberger et al.[28] for both monomeric and dimeric iron sites. Furthermore, the role of NO_2 during NH_3-SCR has not been investigated in the present study, and therefore, NO oxidation is not included in the SCR simulation.

An overconsumption of ammonia during NH_3-SCR over Fe-zeolites has previously been observed by Sjövall et al.[25] Furthermore, Nedyalkova et al.[30] showed, using isotopic labeled experiments, that this overconsumption is due to so-called parasitic NH_3 oxidation. In the present model, the stoichiometry between NO and NH_3 during NH_3-SCR is 1:1. The effect of NH_3 overconsumption can be observed in Figures 1b and 2, where the simulated outlet concentration of NH_3 is slightly higher than the experimental outlet level, especially at the lower temperatures ($T < 400$°C) where the NH_3 conversion is not complete. This discrepancy was, by Sjövall et al.[25] compensated by changing the stoichiometry of the SCR reaction in the model. However, in the present model the stoichiometry was kept at 1:1.[16]

Furthermore, since the development of our previous deactivation model of Fe-BEA[16] recent results[14] have provided new details regarding the ratio between the iron sites. Hence all pre-exponential factors, A_i, used in the previous model of Fe-BEA for NH_3- and NO adsorption and desorption, NH_3- and NO oxidation, and NH_3-SCR are recalculated using the new site densities of the different iron species. However, the pre-exponential factor for the spillover rate (Reaction 6 in Supporting Information, S1) was previously found to be constant, and therefore, not recalculated. A summary of all reaction rates and parameters can be found in Section S1 of the Supporting Information.

For a more thorough description of the kinetic model and assumptions, reaction rates and parameter fitting, see Ref. 16.

Results and Discussion

NH_3 storage

To describe the changes in ammonia storage capacity after phosphorous exposure for 14 and 24 h, the density of sites for weakly bound ammonia, W, had to be significantly decreased, whereas the number of Brønsted sites, $Z_{Br,1}$, had to be increased for the poisoned samples. However, for the sample exposed for 48 h, the site density was not significantly changed compared to the fresh sample. Furthermore, due to the difference in ammonia desorption maximum for the phosphorous-exposed Fe-BEA samples, the desorption energy for ammonia adsorbed on Brønsted sites, $Z_{Br,1}$, was slightly changed in the model to fit the experiments well for the poisoned samples indicating that the initially formed phosphorous pentoxides block sites for loosely bound ammonia and create new sites for more strongly bound NH_3. However, the decrease in activation energy indicates that

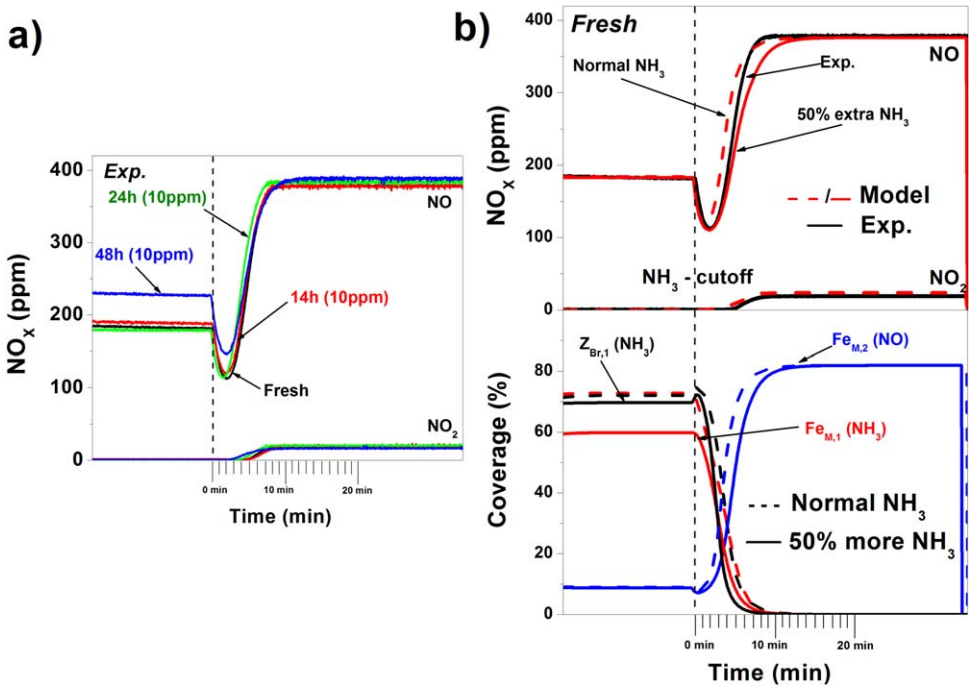

Figure 3. Evolution of NO and NO_2 concentrations during ammonia inhibition experiments over Fe-BEA.

(a) Catalysts exposed to 10 ppm H_3PO_4 for 14, 24, and 48 h compared to a fresh sample. (b) Measured and calculated NO and NO_2 outlet concentrations during NH_3 inhibition experiments for the fresh Fe-BEA. The samples were exposed to 400 ppm NO, 400 ppm NH_3, 8% O_2, and 5% H_2O at 250°C for 40 min. After 40 min, the gas mixture was kept unchanged except the NH_3 gas feed which was cut off. The activity was continuously measured before and after the ammonia cut off. The total flow rate was 3500 ml/min and Ar was used as balance. [Color figure can be viewed in the online issue, which is available at wileyonlinelibrary.com.]

ammonia bound to the new site is less strongly bound than NH_3 on Brønsted sites in the zeolite

The ammonia storage sites in zeolite BEA can be described by up to 16 adsorption sites with different adsorption energies, as shown previously by Pinto et al.[31] However, it was discussed that the main ammonia desorption peak can be simplified and described by desorption from two main storage sites with different binding energies to ammonia.[29,31] This has recently been further studied by our group,[18] where the NH_3 desorption peak was modeled using two main storage sites in the zeolite with different binding energy to ammonia. Further discussions about the simplifications made for the ammonia storage capacity in the kinetic deactivation model are found in Refs. 16,18. However, in our previous study of phosphorous-exposed Fe-BEA, it was found by XPS measurements that phosphorous pentoxides are formed initially on the surface, when the catalyst is exposed to phosphorous (14 and 24 h). Longer time of phosphorous exposure (48 h) results in increased relative amount of metaphosphates.[14] The relative concentration of metaphosphates was higher than the concentration of phosphorous pentoxides after 48 h of phosphorous exposure. These results can explain the shift of the ammonia desorption maximum toward lower temperatures for the samples exposed to phosphorous for 14 and 24 h. These results indicate that the formed phosphorous pentoxides primarily block the stronger acid sites of the two ammonia storage sites as proposed by Pinto et al.,[31] creating new sites with slightly lower binding energy to NH_3, which results in an overall lower binding energy of ammonia in the system. Furthermore, the shift back of the ammonia desorption maximum toward higher temperature after 48 h of phosphorous exposure might be due to that the formed metaphosphates decrease the relative concentration of phosphorous pentoxides blocking the stronger acid sites in the zeolite.

For the ammonia adsorption results, see the Supporting Information (S2). The changes in site density and binding energy due to phosphorous exposure are summarized in Table 1.

NO adsorption

The kinetic parameters and site densities for NO adsorption for fresh and phosphorous-exposed Fe-BEA are fitted from NO-TPD experiments. For the iron site, adsorption of NO was fitted for the monomeric iron site, $Fe_{M,2}$. However, the kinetic parameters and the density for the Brønsted site, $Z_{Br,2}$, are used from our previous deactivation model for the zeolite,[16] and thus, not changed when modeling the effect of the adsorption of NO. The NO storage model describes the experiments well for fresh and phosphorous exposed Fe-BEA by decreasing the density of the monomeric iron site $Fe_{M,2}$. The results show that the site density of $Fe_{M,2}$, decreases significantly after 48 h compared to 14 and 24 h phosphorous exposure. Furthermore, note that $Fe_{M,1}$ and $Fe_{M,2}$, represent the same type of site, and therefore, equally and simultaneously decreased. As previously mentioned, XPS results from our previous study of phosphorous-exposed Fe-BEA[14] showed a significant increase in the relative concentration of metaphosphates over the Fe-BEA samples after 48 h of phosphorous exposure. This may indicate that the formed metaphosphates hinder NO adsorption on iron sites, which could explain the significant decrease in site density of $Fe_{M,2}$, after 48 h in the model required to fit the

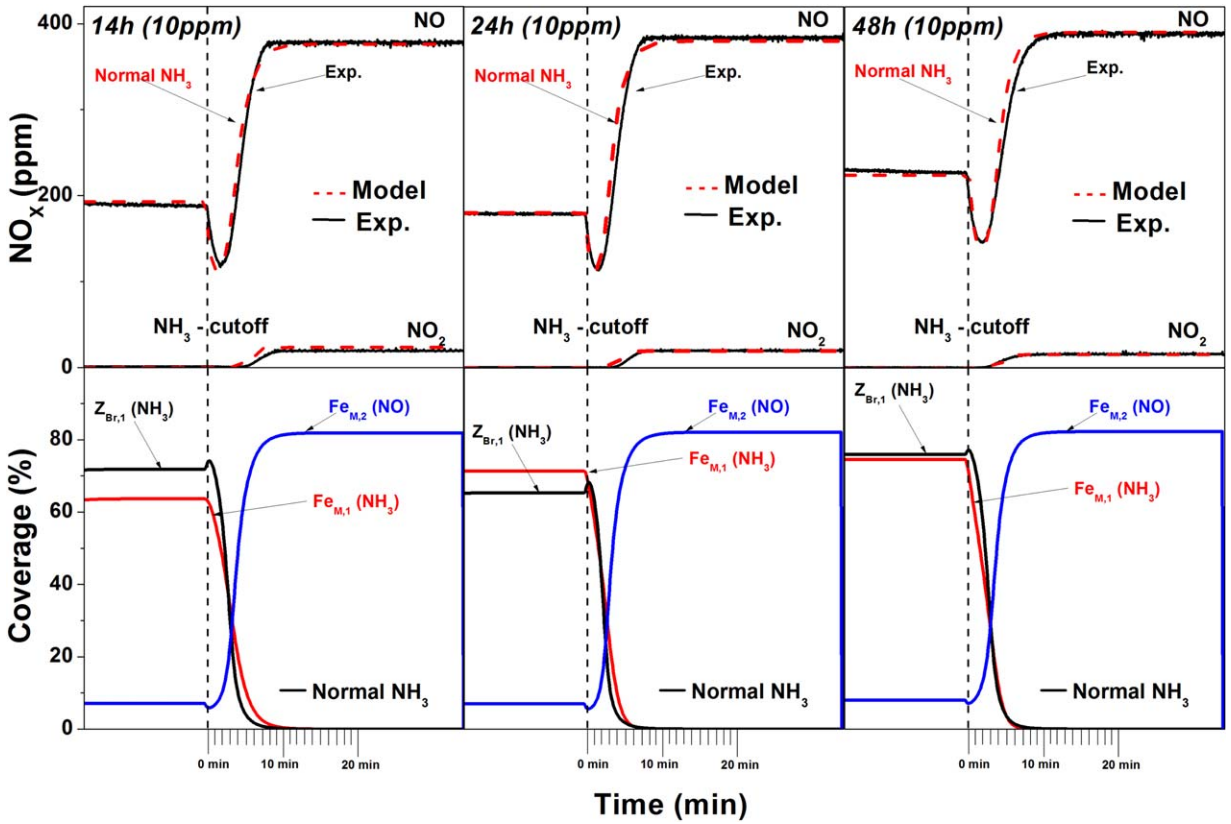

Figure 4. Measured and calculated NO and NO_2 outlet concentration during NH_3 inhibition experiments for all Fe-BEA samples exposed to 10 ppm of H_3PO_4 with the surface coverage of NO and NH_3 over sites, $Z_{Br,1}$, $Fe_{M,1}$, and $Fe_{M,2}$.

[Color figure can be viewed in the online issue, which is available at wileyonlinelibrary.com.]

experiments well. The site densities for all samples are summarized in Table 1.

NH_3 and NO oxidation

Similar to the previous reaction steps, the kinetic parameters for NH_3- and NO-oxidation, and the site density for the Brønsted site, $Z_{Br,2}$, are used from our previous deactivation model for the zeolite[16] and kept constant for the simulations of both fresh and phosphorous-exposed Fe-BEA samples.

Brandenberger et al.[28] showed a clear linear correlation between the concentration of dimeric iron species and the activity for ammonia oxidation over Fe-ZSM-5. The ammonia oxidation over the phosphorous-exposed samples, in the present study, shows a significant decrease in activity at higher temperatures (400 and 500°C), especially after 48 h of exposure, thus the site density for the dimeric iron sites is decreased.

The density of iron particle sites, Fe_P, in the model for Fe-BEA had to be decreased in the simulations to fit the corresponding experiment. However, the NO oxidation experiments show a more continuous decrease in activity, compared to the other activity tests, and therefore, it cannot be ruled out that the phosphorous pentoxides initially formed after 14 h exposure also may block the iron particle sites. The NH_3-oxidation simulation shows a more significant decrease after 48 h of phosphorous exposure indicating that the metaphosphates block the dimeric iron sites, whereas these sites are not significantly affected by the phosphorous pentoxides.

For the NH_3- and NO-oxidation results, see Supporting Information (S2). The changes in density for the dimeric iron and iron particle are summarized in Table 1 for all samples.

NH_3-SCR

The objective of this study is to investigate whether a previously developed kinetic deactivation model for NH_3-SCR over Fe-BEA can describe phosphorous deactivation of this type of catalyst. Furthermore, the focus is to describe the dynamics of the active iron species, and therefore, fast SCR conditions are avoided and hence NO_2 is not included in the SCR reaction. The NO-oxidation reaction step was, therefore, not included in the SCR simulations.

Figure 1a shows the effect of phosphorous exposure on the SCR activity. At lower reaction temperatures (200–300°C), the SCR activity over Fe-BEA is observed to be more affected by phosphorous exposure compared to higher temperatures (400–500°C). However, at high temperatures, the conversion is almost complete, and it is, therefore, more difficult to quantify the deactivation. Figure 1b, shows the simulated and experimental outlet concentrations of NO and NH_3 for the fresh Fe-BEA catalyst during NH_3-SCR together with the calculated mean coverage of adsorbed NO and NH_3 on Brønsted sites, $Z_{Br,2}$, and monomeric iron sites, $Fe_{M,1}$ and $Fe_{M,2}$. All previously fitted kinetic parameters for NH_3- and NO-TPD, NH_3-oxidation and site densities are included in the model together with the NH_3-SCR reactions.

Table 2. Experimental and Simulated Steady State NO_X Conversions Between 150 and 500°C for the Samples Exposed to 10 ppm of H_3PO_4

	NO_X conversion (%)					
Sample	150°C	200°C	250°C	300°C	400°C	500°C
Fresh (exp.)	4.3	20	61	87	96	99
Fresh (sim.)	3.0	18	61	89	97	98
14 h (exp)	3.5	18	55	84	93	97
14 h (sim)	2.3	16	54	84	94	97
24 h (exp.)	0.5	17	55	83	92	95
24 h (sim.)	2.3	16	53	83	93	96
48 h (exp)	1.2	14	46	81	93	95
48 h (sim)	1.2	14	46	80	93	96.

The model is able to describe the NH_3-SCR experiments well over the entire temperature interval studied. As previously mentioned, for temperatures up to 300°C the monomeric iron species provide the main active site for the SCR reaction, while for temperatures above 400°C, the experimental results for NO reduction cannot solely be described by reaction over the monomeric iron sites, hence the NO reduction proceeds primarily over dimeric iron sites at higher temperatures. As previously shown for the same type of catalyst,[15,16] a large fraction of the active sites in the catalyst is not used at high temperatures (>400°C) due to high reaction rates. At 400°C, Auvray et al.[32] showed that only 1/8 of the catalyst length is used for NH_3-SCR over Cu-BEA using spatially resolved MS measurements. Hence, to observe a significant decrease in NO_X reduction at high temperatures, a strong deactivation with a considerable loss of active iron sites must proceed.

Between 250 and 300°C as well as between 300 and 400°C, an increased NO reduction can be observed during the temperature ramp, which is described well by the model. The increased NO reduction can be correlated with the NO and NH_3 coverages shown in Figure 1b, where the latter is affected by ammonia spillover. The adsorbed ammonia on the Brønsted sites, $Z_{Br,1}$, starts to desorb during the temperature ramps buffering the monomeric iron sites, $Fe_{M,1}$, whereby the surface concentration of ammonia over $Fe_{M,1}$ increases, hence the increased NO conversion. As previously mentioned, a more detailed description of the spillover mechanism used can be found in Ref. 16. Figure 2, shows the simulated and experimental outlet concentrations of NO and NH_3 for the phosphorous-exposed Fe-BEA samples during NH_3-SCR together with the calculated mean coverage of the adsorbed species. The fitted kinetic parameters from the fresh sample are kept constant and the previously achieved changes in site densities for the poisoned samples during NH_3-TPD and NH_3 oxidation are applied to the SCR experiment for the phosphorous-exposed samples. The decrease in site density for the dimeric iron sites is taken from the NH_3-oxidation experiments while the decrease of the monomeric iron sites is fitted using the NO-TPD experiments together with the NH_3-SCR experiments.

In general, the model predicts the SCR activity well by decreasing the density of the active sites. It can be noted that the decrease in relative amount is higher for dimeric iron species than for monomeric iron species, indicating higher sensitivity toward phosphorous exposure for the former species. However, the decrease in dimeric iron species does not affect the NO conversion, which is in agreement with the results by Auvray et al.,[32] indicating that the deactivation at higher temperatures needs to be more severe to have a significant impact on the SCR reaction. Furthermore, the results show that the monomeric iron species are not as sensitive to phosphorous as the dimeric iron species but the negative impact of phosphorous exposure on the SCR activity at lower temperatures is higher for the monomeric iron sites. It should be added that in a study by Silver et al.,[27] it was shown that there is a temperature dependence of the ageing of Fe-zeolites due to phosphorous exposure. However, in this study, the phosphorous exposure was performed at constant temperature, and therefore, possible effects of the temperature of poisoning were not included.

The experimental steady state NO_X conversions for the fresh sample and for the samples exposed to 10 ppm of phosphorous are summarized in Table 2 and compared to the corresponding results from the simulations. The decrease in number of sites in the model is summarized in Table 1 for all samples.

Ammonia inhibition

The deactivation model was further validated using ammonia inhibition experiments during SCR for both fresh and phosphorous-exposed samples. Ammonia inhibition experiments were performed during NH_3-SCR conditions at 250°C. After 40 min with constant gas composition, the ammonia supply was instantly cut off while the SCR activity was continuously measured for another 40 min. Figure 3a, shows the experimental results for the inhibition experiment at 250°C, where fresh and phosphorous exposed samples are compared. A clear difference in increased NO reduction after ammonia cut off between the different samples can be observed. For the fresh Fe-BEA sample, the period with increased NO reduction is about 4 min (until it passes the same level as before the NH_3 cut off). The trend is similar for the Fe-BEA samples exposed to phosphorous for 14 h, where the increased NO reduction period does not significantly decrease. However, for the samples exposed to phosphorous for 24 and 48 h, the increased NO reduction period is about 3 and 5 min, respectively. The reason for the longer period with increased NO reduction for the sample exposed to phosphorous for 48 h, compared to 24 h, is that the activity is significantly lower; hence it takes longer time to consume the stored ammonia. The fitted deactivation model, with all parameters kept unchanged, was applied directly to simulate the ammonia inhibition experiments. Furthermore, due to observed NO_2 production after the ammonia cut off, the reaction steps for NO oxidation were included in the reaction just after the NH_3 cut off to validate the steady state level of NO and the amount of NO_2 produced.

Figure 3b, shows the experimental and simulated outlet concentrations of NO and NO_2 for the fresh Fe-BEA sample together with calculated coverage of adsorbed NO and NH_3. The solid red lines show the simulated results directly applied to the corresponding experimental results without any changes in site density. It can be observed that the calculated inhibition period is slightly shorter compared to the experiments, indicating a deficit of ammonia buffering the active iron sites. The model only takes into account ammonia spillover from the main Brønsted site, $Z_{Br,1}$, to the monomeric iron site, $Fe_{M,1}$, while more ammonia is assumed to adsorb on the weak adsorption site, W, which is not assumed to spillover in the present model. Thus, this can explain the deficit of ammonia, which can spillover to the monomeric iron sites. If the amount of strongly bound ammonia is increased by

50%, by increasing the density of the main Brønsted site, $Z_{Br,1}$, the increased NO reduction period fits well with the experiment, marked as the dashed red line in Figure 3b. The increase in ammonia storage in the model can be regarded to represent the nonparticipating ammonia (in the SCR reaction) from the weaker storage sites. As previously mentioned, the adsorption of ammonia over H-BEA can be described by a relatively high number of different adsorption sites[31] where the binding energy varies from 50 to 325 kJ/mol. If the model would have included stronger acid sites for NH_3 adsorption, releasing ammonia slower or a spillover between weakly and strongly bound ammonia, the deficit in the amount of ammonia participating in the SCR reaction could be lower. However, the nature of the different adsorption sites for ammonia in the zeolite structure is still unclear, hence the model is simplified to include only one type of Brønsted site (Z_{Br}) responsible for desorption of ammonia from the strong Brønsted acid sites. The model describes the dynamics of the adsorbed species well after the ammonia cut off, when the amount of stored ammonia is increased with 50% for the fresh Fe-BEA sample. The same results were found when simulating the experiments over the deactivated Fe-BEA samples after hydrothermal treatment as well.[16] The ammonia storage capacity had to be increased by 50% for the hydrothermally deactivated samples to compensate for the ammonia deficit. Furthermore, the lower panel of Figure 3b shows the change in coverage for the adsorbed species before and after the ammonia storage is changed. It can be observed that the increase in ammonia storage does not affect the coverage of NO, hence the steady state reduction of NO is not changed. This agrees well with other studies,[1,33] concluding no need of high density of Brønsted acid sites to achieve high activity for the NH_3-SCR reaction.

Figure 4 shows the experimental and simulated outlet concentrations of NO and NO_2 for the phosphorous-exposed Fe-BEA samples together with the coverage of adsorbed species on the iron sites. Contrary to the fresh sample, it can be noted that there is no need for an increase of the ammonia storage capacity to simulate the increased NO reduction for the phosphorous-exposed samples. If assuming that the previous deficit in ammonia may be due to that the sites with weakly adsorbed NH_3 are not included in the spillover of ammonia or because of the simplification of the ammonia storage using one main storage site in the model, these results show that this is not the case for the phosphorous-exposed samples. This indicates that the phosphorous species formed on the surface hinder the local transport of ammonia between storage sites. If the local ammonia transport in the zeolite would have been unchanged after phosphorous exposure, the same deficit in ammonia should have been observed as for the fresh sample. This indicates that the decreased ammonia transport in the zeolite due to formed phosphorous species results in decreased SCR performance during transient conditions. It is worth to note that in applications with varying NH_3 feed, ammonia buffer capacity is advantageous.

Concluding Remarks

The objective of this study was to investigate whether a previously developed microkinetic deactivation model for NH_3-SCR over hydrothermally treated Fe-BEA can be applied to describe chemical deactivation of this type of catalyst due to phosphorous exposure. The focus was to validate the previously proposed chemical deactivation mechanism of blocking active iron sites due to formation of phosphorous species on the surface using the microkinetic deactivation model. Three different types of iron sites are included in the model; monomeric and dimeric iron species, and Fe_2O_3 particles. The monomeric iron species provide the governing site for low-temperature SCR, while the dimeric iron species provide the governing site for high-temperature SCR and NH_3-oxidation, and Fe_2O_3 particles are active for oxidation of NO. Furthermore, the Brønsted sites in the zeolite are responsible for the main storage of strongly bound ammonia in the catalyst. In addition, a mechanism for spillover of ammonia adsorbed on Brønsted sites to monomeric iron sites is also included in the model to account for transient conditions. The NH_3-SCR model combines three subsystems describing; (1) the adsorption of NH_3 and NO on the Brønsted and monomeric iron sites, (2) the oxidation of ammonia and NO, while the third subsystem (3) accounts for the SCR reactions.

The microkinetic deactivation model was used to describe the decreased activity of Fe-BEA due to phosphorous exposure. The kinetic parameters were used from the originally developed model except for the site densities, which were fitted to the experiments used in this work, and the pre-exponential factors that were recalculated for the reaction over iron sites due to the more well-determined ratio between the iron sites provided recently. The deactivation was simulated by decreasing the number of active sites due to formation of metaphosphates blocking the active iron sites.

In summary, the kinetic deactivation model originally developed for hydrothermally treated samples describes the experiments for phosphorous-exposed Fe-BEA well. Furthermore, the desorption energy of ammonia adsorbed on the Brønsted sites had to be slightly changed for the phosphorous-exposed samples. This is in accordance with our previous studies where the simplified Brønsted site in the present model may be described by two sites with different NH_3 binding energies. The results indicate that the deactivation rate due to phosphorous exposure is different for the two sites, shifting the position of the overall desorption peak of ammonia. Furthermore, the results show that the reaction rate for low-temperature SCR is very sensitive to the decreased density of monomeric iron sites, while the SCR reaction at higher temperatures is not that sensitive to deactivation of dimeric iron species, due to the high reaction rates. This is in accordance with other studies showing that at high temperatures only a fraction of the catalyst is used, hence a more severe deactivation is required to observe any significant decrease in activity. Due to the simplified spillover model, where weakly bound ammonia is not included, the simulations indicate a deficit of ammonia for fresh Fe-BEA but not for the phosphorous-exposed samples. Hence, it is suggested that the exposure to phosphorous may affect the internal transport of ammonia between the ammonia storage sites buffering the active iron sites, resulting in lower SCR performance during transient conditions.

Acknowledgments

This work has been performed within the FFI program (Proj. No. 32900-1), which is financially supported by the Swedish Energy Agency and partly within the Competence Centre for Catalysis, which is hosted by Chalmers University

of Technology and financially supported by the Swedish Energy Agency and the member companies AB Volvo, ECAPS AB, Haldor Topsøe A/S, Scania CV AB and Volvo Car Corporation AB. Financial support from Knut and Alice Wallenberg Foundation, Dnr KAW 2005.0055, is gratefully acknowledged. The authors would also like to thank Volvo Group Trucks Technology and Miroslawa Milh for help with the chemical deactivation of the samples.

Literature Cited

1. Brandenberger S, Krocher O, Tissler A, Althoff R. The state of the art in selective catalytic reduction of NO_x by ammonia using metal-exchanged zeolite catalysts. *Catal Rev-Sci Eng*. 2008;50(4):492–531.
2. Sjövall H, Olsson L, Fridell E, Blint RJ. Selective catalytic reduction of NO_x with NH_3 over Cu-ZSM-5—the effect of changing the gas composition. *Appl Catal B*. 2006;64(3–4):180–188.
3. Rahkamaa-Tolonen K, Maunula T, Lomma M, Huuhtanen M, Keiski RL. The effect of NO_2 on the activity of fresh and aged zeolite catalysts in the NH_3-SCR reaction. *Catal Today*. 2005;100(3–4):217–222.
4. Kieger S, Delahay G, Coq B, Neveu B. Selective catalytic reduction of nitric oxide by ammonia over Cu-FAU catalysts in oxygen-rich atmosphere. *J Catal*. 1999;183(2):267–280.
5. Park JH, Park HJ, Baik JH, et al. Hydrothermal stability of CuZSM5 catalyst in reducing NO by NH_3 for the urea selective catalytic reduction process. *J Catal*. 2006;240(1):47–57.
6. Sullivan JA, Cunningham J, Morris MA, Keneavey K. Conditions in which Cu-ZSM-5 outperforms supported vanadia catalysts in SCR of NO_x by NH_3. *Appl Catal B*. 1995;7(1–2):137–151.
7. Sjövall H, Fridell E, Blint R, Olsson L. Identification of adsorbed species on Cu-ZSM-5 under NH_3 SCR conditions. *Top Catal*. 2007;42–43(1):113–117.
8. Grossale A, Nova I, Tronconi E, Chatterjee D, Weibel M. The chemistry of the NO/NO_2-NH_3 "fast" SCR reaction over Fe-ZSM5 investigated by transient reaction analysis. *J Catal*. 2008;256(2):312–322.
9. Grossale A, Nova I, Tronconi E. Study of a Fe-zeolite-based system as NH_3-SCR catalyst for diesel exhaust aftertreatment. *Catal Today*. 2008;136(1–2):18–27.
10. Kröcher O, Devadas M, Elsener M, Wokaun A, Söger N, Pfeifer M, Demel Y, Mussmann L. Investigation of the selective catalytic reduction of NO by NH_3 on Fe-ZSM5 monolith catalysts. *Appl Catal B*. 2006;66(3–4):208–216.
11. Grossale A, Nova I, Tronconi E. Role of nitrate species in the "NO(2)-SCR" mechanism over a commercial Fe-zeolite catalyst for SCR mobile applications. *Catal Lett*. 2009;130(3–4):525–531.
12. Forzatti P, Lietti L, Nova I, Tronconi E. Diesel NO_x aftertreatment catalytic technologies: analogies in LNT and SCR catalytic chemistry. *Catal Today*. 2010;151(3–4):202–211.
13. Kamasamudram K, Currier NW, Chen X, Yezerets A. Overview of the practically important behaviors of zeolite-based urea-SCR catalysts, using compact experimental protocol. *Catal Today*. 2010;151(3–4):212–222.
14. Shwan S, Jansson J, Olsson L, Skoglundh M. Chemical deactivation of Fe-BEA as NH_3-SCR catalyst—effect of phosphorous. *Appl Catal B*. 2014;147:111–123.
15. Shwan S, Nedyalkova R, Jansson J, Korsgren J, Olsson L, Skoglundh M. Hydrothermal stability of Fe-BEA as SCR-catalyst. *Ind Eng Chem Res*. 2012;51:12762–12772.
16. Shwan S, Jansson J, Korsgren J, Olsson L, Skoglundh M. Kinetic modeling of H-BEA and Fe-BEA as NH_3-SCR catalysts—effect of hydrothermal treatment. *Catal Today*. 2012;197(1):24–37.
17. Shwan S, Adams E, Jansson J, Skoglundh M. Effect of thermal ageing on the nature of iron species in Fe-BEA. *Catal Lett*. 2013;143(1):43–48.
18. Shwan S, Nedyalkova R, Jansson J, Korsgren J, Olsson L, Skoglundh M. Influence of hydrothermal ageing on NH_3-SCR over Fe-BEA—inhibition of NH_3-SCR by ammonia. *Top Catal*. 2013;56(1–8):80–88.
19. Nedyalkova R, Shwan S, Skoglundh M, Olsson L. Improved low-temperature SCR activity for Fe-BEA catalysts by H_2-pretreatment. *Appl Catal B*. 2013;138–139:373–380.
20. Bartholomew CH. Mechanisms of catalyst deactivation. *Appl Catal A*. 2001;212:17–60.
21. AVL BOOST. Aftertreatment manual: AVL. Available at: www.avl.com, Last accessed on 2014.
22. Shwan S, Partridge W, Choi JS, Olsson L. Kinetic modeling of NO_x storage and reduction using spatially resolved MS measurements. *Appl Catal B*. 2014;147:1028–1041.
23. Olsson L, Sjövall H, Blint RJ. A kinetic model for ammonia selective catalytic reduction over Cu-ZSM-5. *Appl Catal B*. 2008;81(3–4):203–217.
24. Malmberg S, Votsmeier M, Gieshoff J, Söger N, Mussmann L, Schuler A, Drochner A. Dynamic phenomena of SCR-catalysts containing Fe-exchanged zeolites—experiments and computer simulations. *Top Catal*. 2007;42–43(1–4):33–36.
25. Sjövall H, Blint RJ, Gopinath A, Olsson L. A kinetic model for the selective catalytic reduction of NO(x) with NH(3) over an Fe-zeolite catalyst. *Ind Eng Chem Res*. 2010;49(1):39–52.
26. Sjövall H, Blint RJ, Olsson L. Detailed kinetic modeling of NH_3 and H_2O adsorption, and NH_3 oxidation over Cu-ZSM-5. *J Phys Chem C*. 2009;113(4):1393–1405.
27. Silver RG, Stefanick MO, Todd BI. A study of chemical aging effects on HDD Fe–zeolite SCR catalyst. *Catal Today*. 2008;136(1–2):28–33.
28. Brandenberger S, Kröcher O, Tissler A, Althoff R. The determination of the activities of different iron species in Fe-ZSM-5 for SCR of NO by NH_3. *Appl Catal B*. 2010;95(3–4):348–357.
29. Hoj M, Beier MJ, Grunwaldt JD, Dahl S. The role of monomeric iron during the selective catalytic reduction of NO(x) by NH(3) over Fe-BEA zeolite catalysts. *Appl Catal B*. 2009;93(1–2):166–176.
30. Nedyalkova R, Kamasamudram K, Currier NW, Li J, Yezerets A, Olsson L. Experimental evidence of the mechanism behind NH_3 overconsumption during SCR over Fe-zeolites. *J Catal*. 2013;299:101–108.
31. Pinto RR, Borges P, Lemos Manda, Lemos F, Védrine JC, Derouane EG, Ramôa Ribeiro F. Correlating NH_3-TPD and H-1 MAS NMR measurements of zeolite acidity: proposal of an acidity scale. *Appl Catal A*. 2005;284(1–2):39–46.
32. Auvray X, Partridge WP, Choi J-S, Pihl JA, Yezerets A, Kamasamudram K, Currier NW, Olsson L. Local ammonia storage and ammonia inhibition in a monolithic copper-beta zeolite SCR catalyst. *Appl Catal B*. 2012;126:144–152.
33. Brandenberger S, Kröcher O, Wokaun A, Tissler A, Althoff R. The role of Brønsted acidity in the selective catalytic reduction of NO with ammonia over Fe-ZSM-5. *J Catal*. 2009;268(2):297–306.

Manuscript received Mar. 18, 2014, and revision received Sep. 10, 2014.